Flight and Full-Scale Wind-Tunnel Comparison

of Pressure Distributions from an F-18

Aircraft at High Angles of Attack

David F. Fisher
NASA Dryden Flight Research Center
Edwards, California

Wendy R. Lanser
NASA Ames Research Center
Moffett Field, California

Abstract

Pressure distributions were obtained at nearly identical fuselage stations and wing chord butt lines in flight on the F-18 HARV at NASA Dryden Flight Research Center and in the NASA Ames Research Center's 80- by 120-ft wind tunnel on a full-scale F/A-18 aircraft. The static pressures were measured at the identical five stations on the forebody, three stations on the left and right leading-edge extensions, and three spanwise stations on the wing. Comparisons of the flight and wind-tunnel pressure distributions were made at $\alpha = 30°$, 45°, and 60°/59°. In general, very good agreement was found. Minor differences were noted at the forebody at $\alpha = 45°$ and 60° in the magnitude of the vortex footprints and a Mach-number effect was noted at the leading-edge extension at $\alpha = 30°$. The inboard leading-edge flap data from the wind tunnel at $\alpha = 59°$ showed a suction peak that did not appear in the flight data. This was the result of a vortex from the corner of the leading-edge flap whose path was altered by the lack of an engine simulation in the wind tunnel.

DRYDEN FLIGHT RESEARCH CENTER

Flight and Full-Scale Wind-Tunnel Comparison of Pressure Distributions from an F/A-18 Aircraft at High Angles of Attack

David F. Fisher
NASA Dryden Flight Research Center
Edwards, California

and

Wendy R. Lanser
NASA Ames Research Center
Moffett Field, California

94-277

Introduction

The High Alpha Technology Program (ref. 1), initiated in 1986, encompasses many research efforts within NASA combining wind-tunnel testing, analytical predictions, piloted simulation, and full-scale flight research. In the program objectives (listed in the figure), full-scale flight validation was essential in developing high-angle-of-attack (high-α) technology. The flight portion of the program at NASA Dryden Flight Research Center focused on the F-18 High Alpha Research Vehicle (HARV), a highly instrumented preproduction F/A-18 aircraft. For the first objective, a new technology that was developed to improve agility at high-α and expand the usable high-α envelope has been thrust vectoring (ref. 2), which is currently being tested on the F-18 HARV. Actuated forebody strakes, ref. 3, soon be tested in flight, may enhance the controllability and maneuverability of the HARV even more. Other similar concepts such as forebody slot blowing have only been tested in the wind tunnel (ref. 4).

The second objective was to "provide flight-validated prediction/analysis methodology including experimental and computational methods that accurately simulate high-angle-of-attack aerodynamics, flight dynamics, and flying qualities" (ref. 1). Definitive surface and off-surface flow visualization (ref. 5) and pressure distribution results from flight (ref. 6) have been used to validate the three-dimensional Navier-Stokes computational fluid dynamics (CFD) solutions obtained for the F/A-18 at high-α for both the steady (ref. 7) and unsteady cases (ref. 8). New techniques in grid generation and flow modeling were developed to simulate the flight results of the highly vortical and separated flows.

Extensive ground testing of 0.06- and 0.16-scale models has been performed at high-α and compared to full-scale flight results (ref. 9). One result of this testing of subscale models is a new method of applying boundary-layer transition strips to the model forebodies to simulate flight results at high-α (refs. 10 and 11). Full-scale tests of an F/A-18 aircraft in the NASA Ames Research Center's 80- by 120-ft wind tunnel have focused on tail buffet, forebody controls, and surface pressures (refs. 4,12, and 13). This paper compares the pressure distributions obtained on the forebody, leading-edge extensions (LEXs), and wings of a full-scale F/A-18 in the wind tunnel with corresponding pressure distributions obtained on the F-18 HARV in 1-g flight. Unlike the subscale model testing, the F/A-18 was tested at slightly higher Reynolds numbers than are generated in flight, though at a slightly lower Mach number. One would expect that these wind-tunnel results would show the best comparison with flight results, especially for those effects for which Reynolds numbers are important.

HAPT Objectives

- Enable expanded high-alpha maneuverability and flight envelopes

- Provide flight-validated high alpha prediction/ analysis methods for superior design methods

Ref. AGARD CP-465, paper #3
Gilbert, Nguyen, Gera

94-278

Test Conditions

Extensive pressure distributions were obtained on the F-18 HARV in flight and on a full-scale F/A-18 in the NASA Ames 80- x 120-ft wind tunnel. Data were obtained over a wide range of angles of attack and sideslip, both in flight and in the wind tunnel. However, only data at $\alpha = 30°$, $45°$, and $60°$ from flight and $\alpha = 30°$, $45°$, and $59°$ from the wind tunnel are presented. The data from the F-18 HARV were obtained in flight at stabilized 1-g conditions between 20,000- and 30,000-ft altitude with the engines set at military power. The Mach numbers (M) in flight ranged from 0.23 to 0.27, while the Reynolds numbers based on wing mean aerodynamic chord ranged from 8.9 to 10 million. Data from the atmospheric wind tunnel were obtained with the full-scale F/A-18 at $M = 0.15$ and a Reynolds number of 12 million. The F/A-18 aircraft was mounted on a three-strut configuration shown in the figure with a production radome, both engines removed, and inlets and exhaust exits open.

Test Conditions
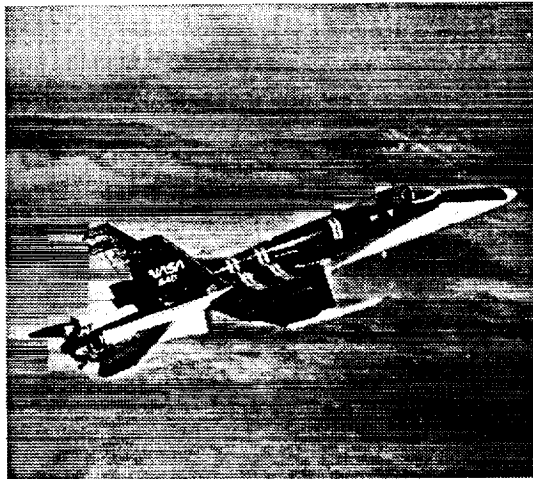
F-18 HARV in flight
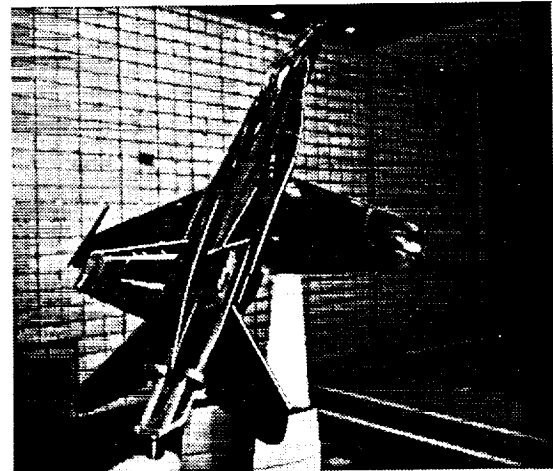
F/A-18 in 18- x 120-ft wind tunnel

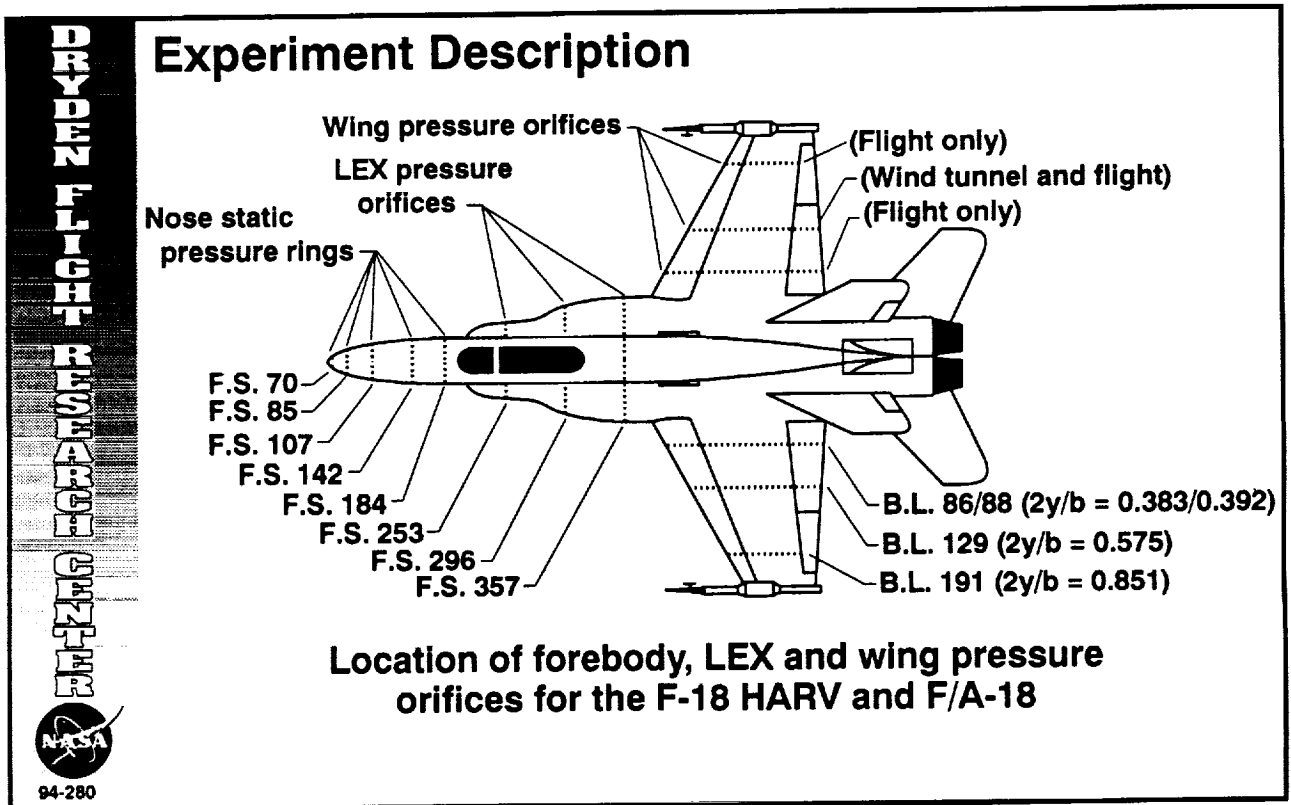DRYDEN FLIGHT RESEARCH CENTER

94-279

Experiment Description

As shown in the figure, pressure distributions were obtained from five circumferential rows of flush orifices on the forebody and three rows of flush orifices on each LEX at identical stations both in flight and in the wind tunnel. Pressure distributions were also obtained on the upper and lower surface of the wings and at three span stations on the left and right wing in flight. In the wind tunnel, pressure distributions were obtained at nearly identical span stations on the left wing and at the midspan location only on the right wing. Flush orifices were installed on the left wing for the wind-tunnel-tested F/A-18 and on the leading-edge flaps of the flight-tested F-18 HARV. On the main wing box and trailing-edge flaps of the F-18 HARV, orifices were drilled in externally installed strip-of-tubing. At W.S. 129 on the left wing of the wind-tunnel experiment, strip-of-tubing was used for data comparison.

Data from the wind tunnel have been corrected for blockage effects using the techniques described in reference 14. The correction for blockage varied with angle of attack. For example, a measured pressure coefficient of -1.0 at $\alpha = 30°$ had a correction of 0.058; at $\alpha = 45°$, a correction of 0.069; and at $\alpha = 59°$, a correction of 0.078.

Experiment Description

Wing pressure orifices
(Flight only)
(Wind tunnel and flight)
(Flight only)

LEX pressure orifices

Nose static pressure rings

F.S. 70
F.S. 85
F.S. 107
F.S. 142
F.S. 184
F.S. 253
F.S. 296
F.S. 357

B.L. 86/88 (2y/b = 0.383/0.392)
B.L. 129 (2y/b = 0.575)
B.L. 191 (2y/b = 0.851)

Location of forebody, LEX and wing pressure orifices for the F-18 HARV and F/A-18

DRYDEN FLIGHT RESEARCH CENTER

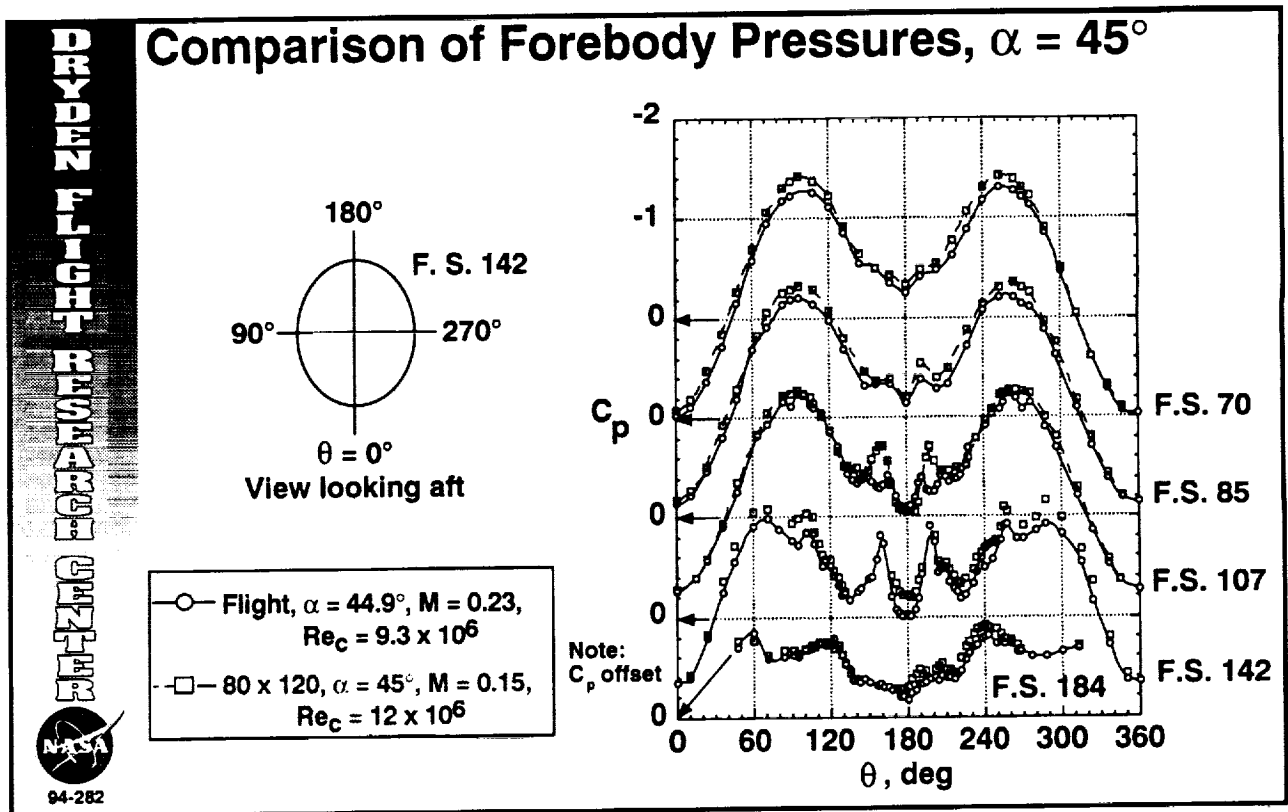94-280

Results and Discussion

Forebody, $\alpha = 30°$

A comparison of the pressure distributions at $\alpha = 30°$ on the forebodies of the F-18 HARV in flight and the F/A-18 in the wind tunnel is shown above. Pressure coefficients from the five rings of static-pressure orifices are plotted as a function of circumferential angle. The points at 0° and 360° correspond with the windward ray and 180° corresponds to the leeward ray. Note that the pressure distribution for each station has been offset and that the arrow points to the corresponding zero-pressure-coefficient axis.

At these conditions the data from flight and the wind tunnel show excellent agreement. The suction peaks at $\theta \approx 100°$ and 260° at F.S. 70 and moving aft to F.S. 142 at $\theta \approx 70°$ and 290° are caused by the acceleration of the flow around the highly curved surface of the forebody. The suction peaks at $\theta \approx 95°$ and 265° at F.S. 142 are the result of an antenna fairing protrusion just forward of the orifice ring. Footprints of the forebody vortex pair can be seen at $\theta \approx 160°$ and 200° at F.S. 142. At this angle of attack the pressure distributions are very symmetrical for all five stations.
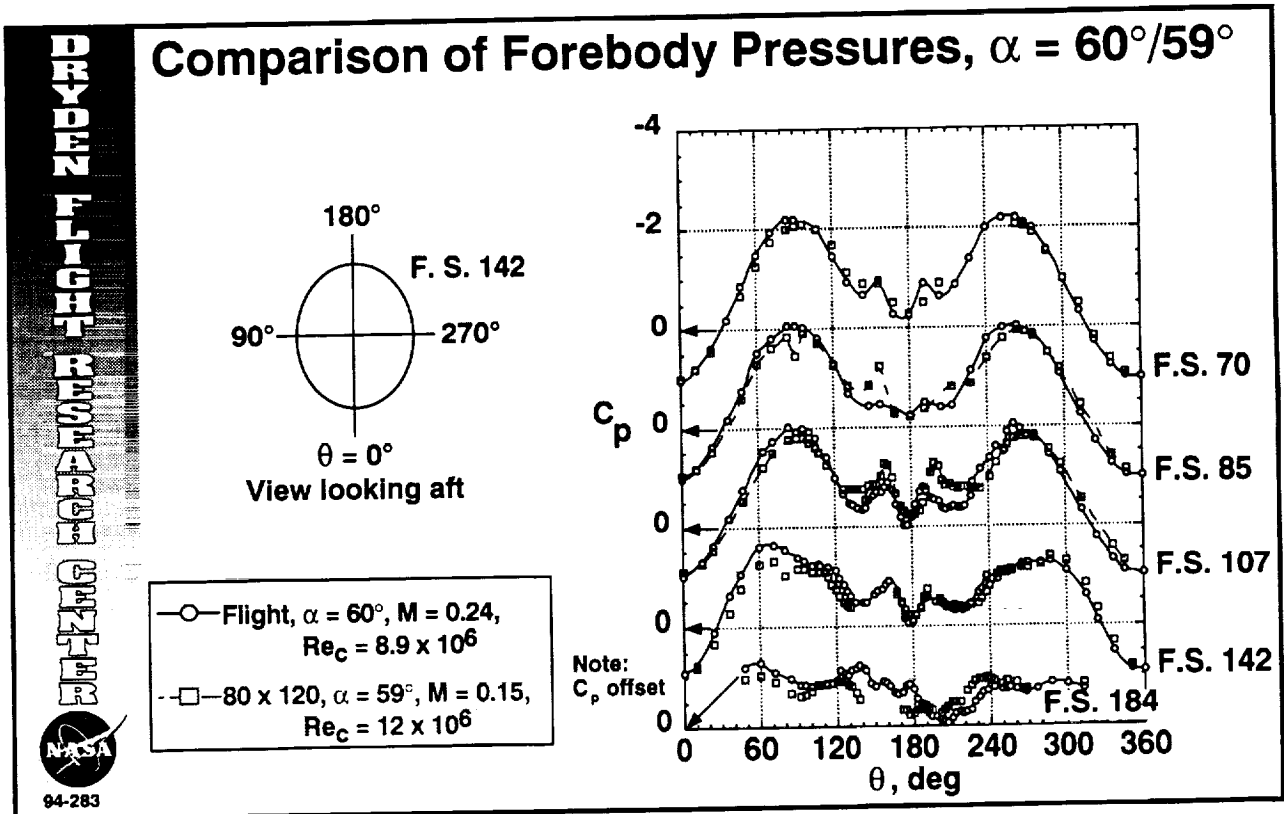

Comparison of Forebody Pressures, $\alpha = 30°$
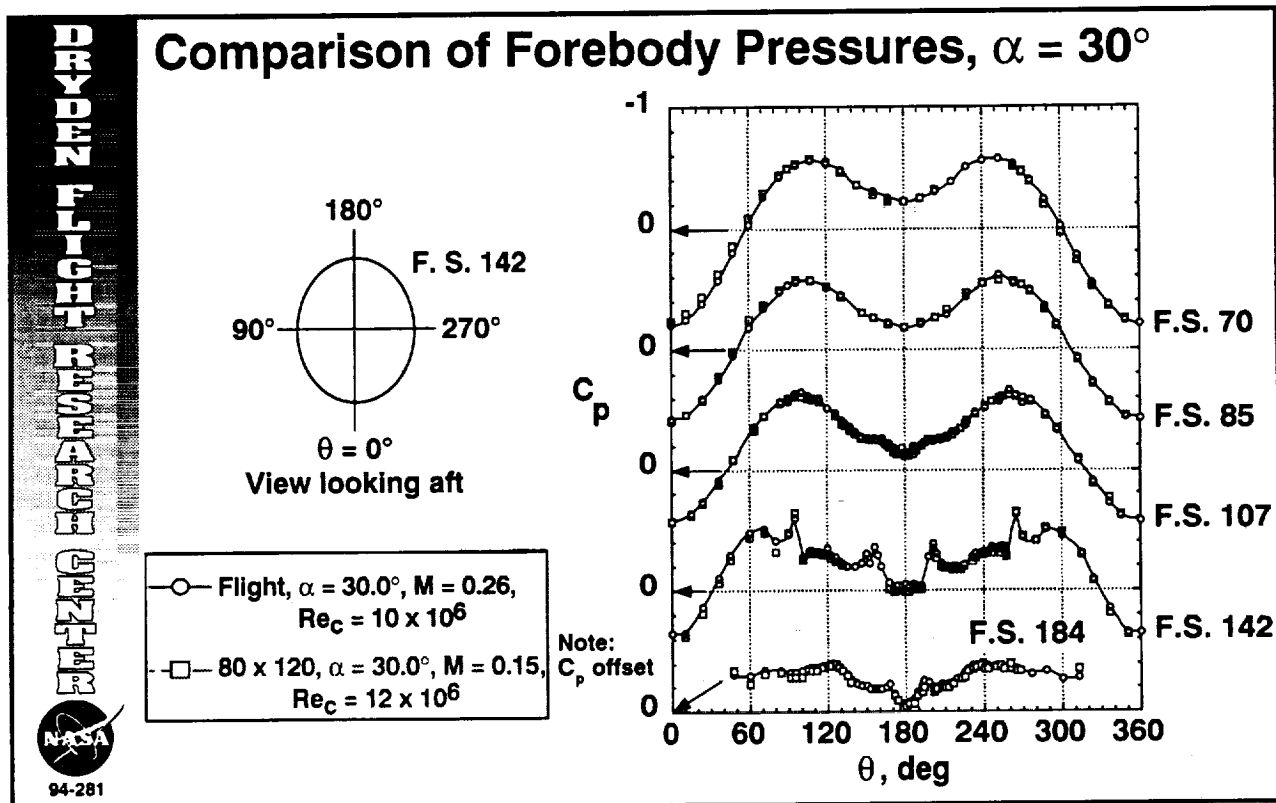
Forebody, $\alpha = 45°$

At 45° angle of attack the suction peaks at $\theta \approx 100°$ and 260° at F.S. 70 and the following stations are more negative for both the flight and wind-tunnel data as compared with the results at $\alpha = 30°$. At F.S. 70 and F.S. 85 the data from the wind tunnel show slightly more negative pressure coefficients than those from flight. At F.S. 107 the suction peaks resulting from the forebody vortex pair from the wind tunnel are significantly more negative than those from flight, while the rest of the pressure distribution shows good agreement. The wind-tunnel data at F.S. 142 and F.S .184 show generally good agreement with the flight data. A slight asymmetry is noted at F.S. 184 for both wind-tunnel and flight data.

Comparison of Forebody Pressures, $\alpha = 45°$

180°

F. S. 142

90° ——|—— 270°

$\theta = 0°$

View looking aft

—O— Flight, $\alpha = 44.9°$, M = 0.23, $Re_c = 9.3 \times 10^6$

- -□- 80 x 120, $\alpha = 45°$, M = 0.15, $Re_c = 12 \times 10^6$

Note: C_p offset

C_p

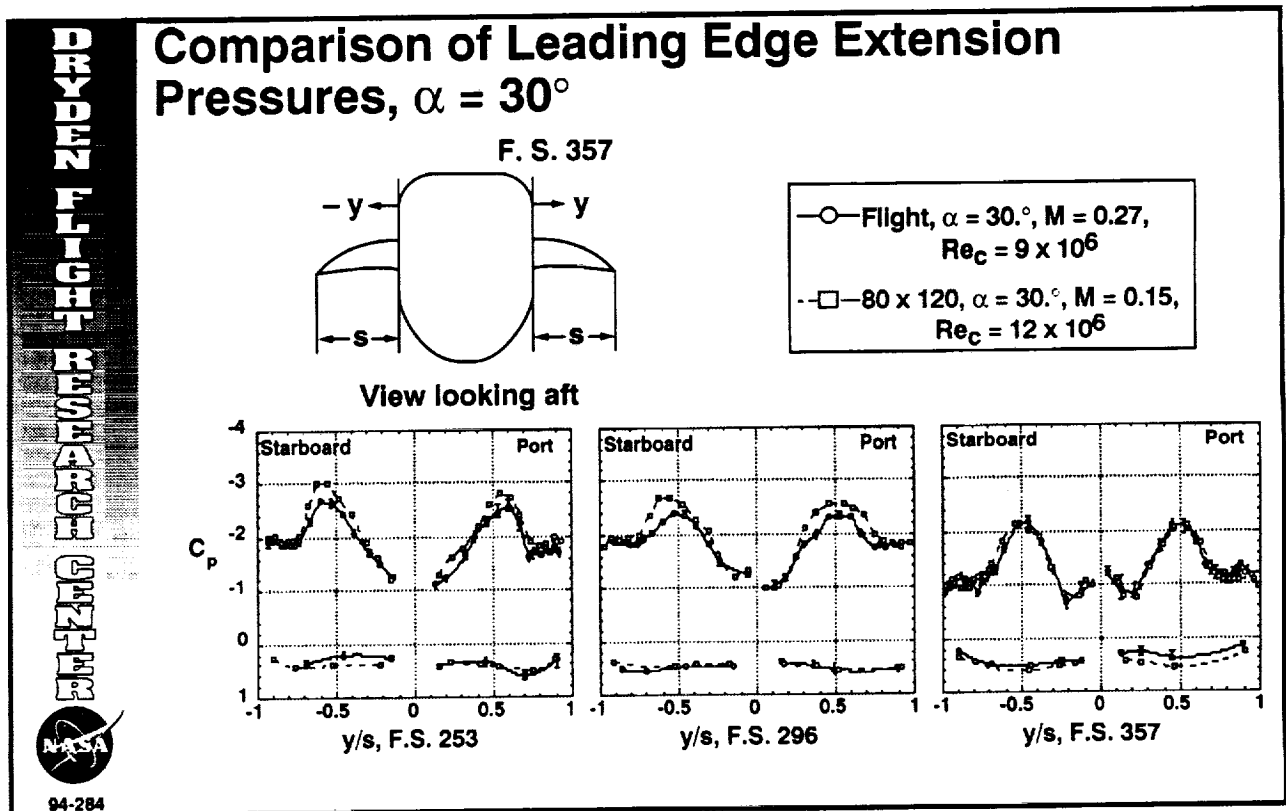F.S. 70

F.S. 85

F.S. 107

F.S. 142

F.S. 184

θ, deg

94-282

Forebody, $\alpha = 60°/59°$

In the figure above, data from the wind tunnel at $\alpha = 59°$ are compared with flight data at $\alpha = 60°$. The angle-of-attack limit in the wind tunnel was 59°. Both the flight and wind-tunnel data show asymmetries in the pressure distributions. This could be the result of slight differences in the surface finish or contour of the forebody between the F-18 HARV and F/A-18 and the presence of a laminar separation bubble (ref. 5) and the difference in the boundary-layer transition location. In reference 15 it was shown that symmetric longitudinal transition strips can reduce forebody asymmetries. The effect of small changes in radome contour was also described in reference 15.
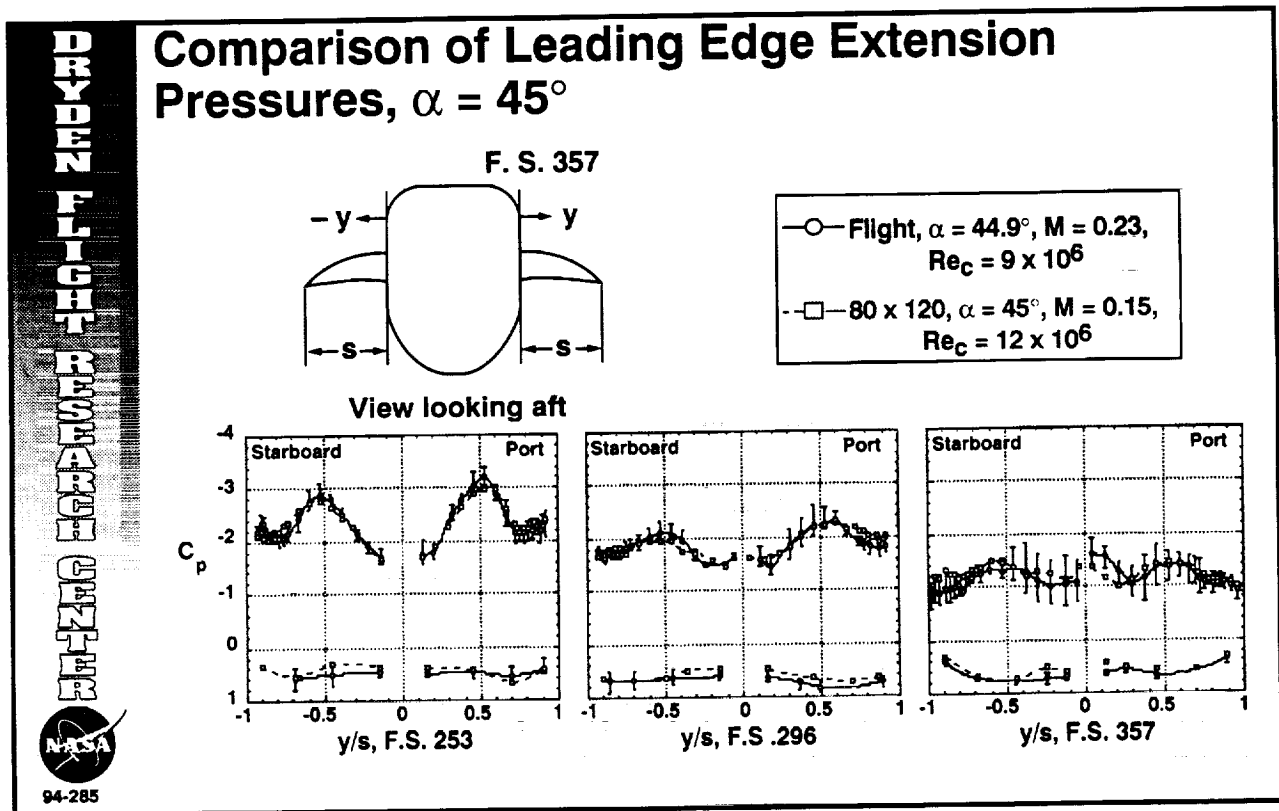

Comparison of Forebody Pressures, $\alpha = 60°/59°$

—O—Flight, $\alpha = 60°$, M = 0.24, $Re_c = 8.9 \times 10^6$

- -□—80 x 120, $\alpha = 59°$, M = 0.15, $Re_c = 12 \times 10^6$

Note: C_p offset

94-283

Leading-Edge Extensions, α = 30°

The figure shows comparisons of the static pressures from identical stations on the LEXs of the F-18 HARV (in flight) and the F/A-18 (in the 80- by 120-ft wind tunnel). These pressure distributions represent only the pressures on the LEXs and not on the fuselage. At this angle of attack the LEX vortex breakdown occurs at approximately F.S. 340 (ref. 16), i.e., between the second and third orifice stations. The static pressures measured below and behind vortex core breakdown tend to be very unsteady. The data from flight are shown with error bars that represent the minimum and maximum values of the 10 samples used to compute the mean. (See the following two figures to see the error bars more clearly.) These pressure fluctuation values are biased in that the transducers were not flush on the surface but sensed the pressures through 0.062-in. diameter tubing that was 1.5 ft long at F.S. 253 and 3.0 ft long at F.S. 357. At this angle of attack the pressure variations from minimum to maximum are relatively small, generally within the size of the symbol. The large suction peaks shown in pressure distributions result from the strong primary vortex shed by the sharp edge of each LEX (ref. 5). The highest suction pressures are at the forward stations and are reduced behind the vortex core breakdown position. At F.S. 253 and 296 the suction peaks in the pressure distributions from the wind tunnel are higher than those from flight. This difference results from the lower Mach number in the wind tunnel, 0.15, as compared with flight, 0.27. This effect of Mach number was shown previously in reference 6 at this angle of attack.

Comparison of Leading Edge Extension Pressures, α = 30°

F. S. 357

—○—Flight, α = 30.°, M = 0.27, $Re_c = 9 \times 10^6$

--□--80 x 120, α = 30.°, M = 0.15, $Re_c = 12 \times 10^6$

View looking aft
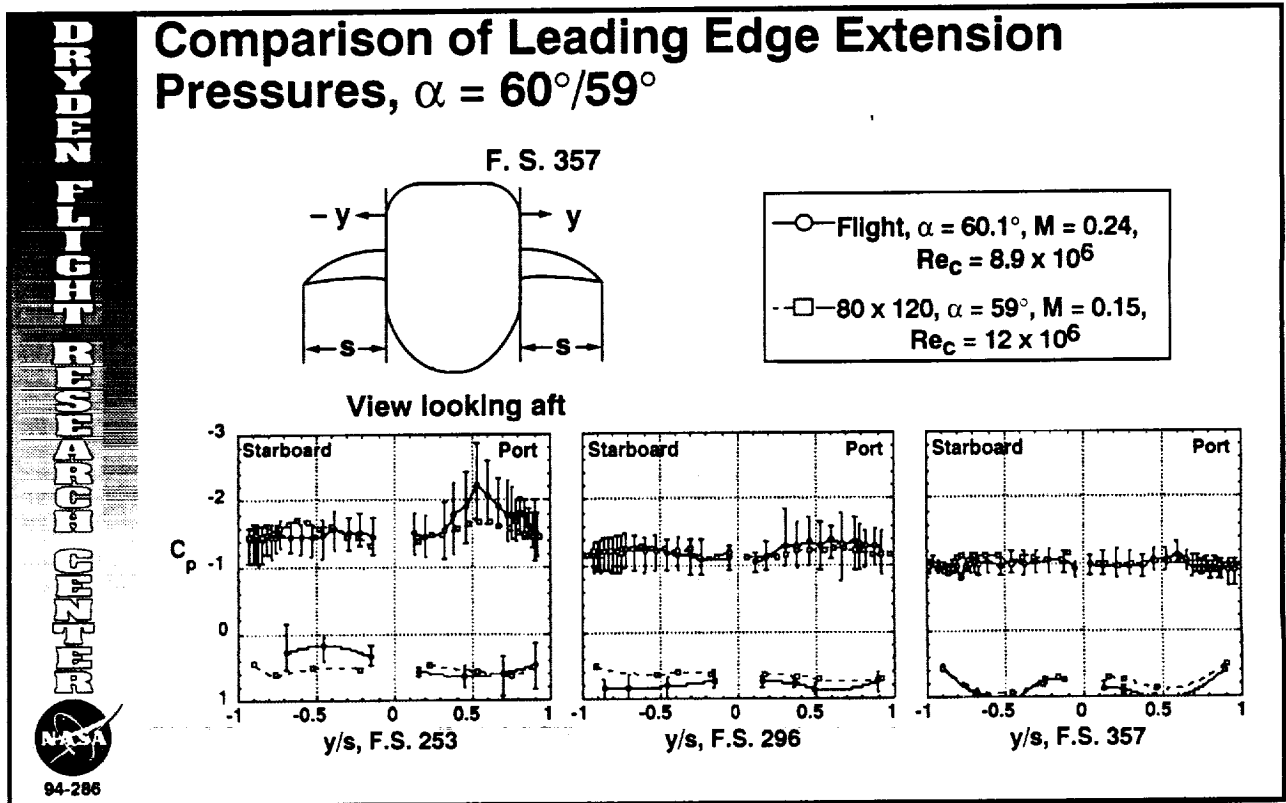
y/s, F.S. 253　　　y/s, F.S. 296　　　y/s, F.S. 357

94-284

Leading-Edge Extensions, $\alpha = 45°$

LEX pressure distributions at an angle of attack of 45° are shown above. At this angle of attack, LEX vortex core breakdown occurs slightly forward of the first orifice station at F.S. 253. Note the reduction and flattening of the suction peaks from the forward orifice station to the aft orifice stations. Also note the large increase in the pressure fluctuations as noted by the length of the error bars for the flight data at this angle of attack as compared with $\alpha = 30°$. At this angle of attack, the wind tunnel data show good agreement with the flight data, even showing similar asymmetries. The effect of Mach number present at $\alpha = 30$ is not noted here.

Comparison of Leading Edge Extension Pressures, $\alpha = 45°$

F. S. 357

−y ← → y

−s → ← s

View looking aft

—○— Flight, $\alpha = 44.9°$, M = 0.23, $Re_c = 9 \times 10^6$

--□-- 80 x 120, $\alpha = 45°$, M = 0.15, $Re_c = 12 \times 10^6$

C_p

Starboard   Port

y/s, F.S. 253

Starboard   Port

y/s, F.S .296

Starboard   Port

y/s, F.S. 357

94-285

Leading-Edge Extensions, α = 60°/59°

The comparison of the LEX pressure distributions at α = 60° from flight and α = 59° from the wind tunnel is shown above. At this angle of attack the LEX vortex cores are completely broken down at the LEX apex and the pressure distributions are generally flat. The pressure fluctuations in the flight data are greatest at the forward station. The wind-tunnel data generally fall well within the band of pressure fluctuations. Some asymmetry is noted, especially at the forward station for the flight data.

Comparison of Leading Edge Extension Pressures, α = 60°/59°

F. S. 357

—○—Flight, α = 60.1°, M = 0.24, $Re_c = 8.9 \times 10^6$

--□--80 x 120, α = 59°, M = 0.15, $Re_c = 12 \times 10^6$

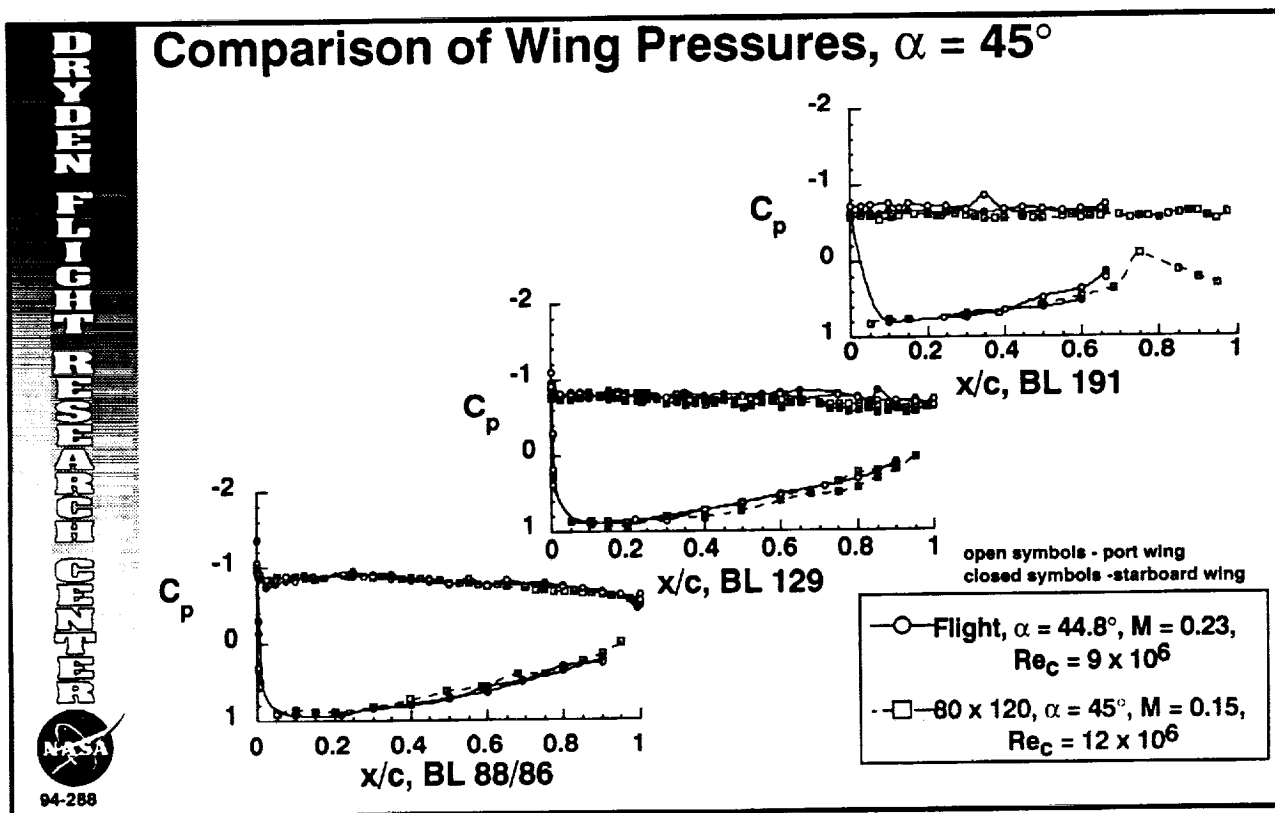**View looking aft**

y/s, F.S. 253

y/s, F.S. 296

y/s, F.S. 357

94-286

Wing, $\alpha = 30°$

Chordwise pressure distributions at $\alpha = 30°$ obtained from the F-18 HARV in flight and F/A-18 in the wind tunnel are shown above. At this angle of attack and higher the 20-percent chord leading-edge flaps are deflected down 33° while the trailing-edge flaps are undeflected. The trailing-edge flaps and ailerons begin at 68-percent chord. Pressure distributions from both the left and right wing are shown for the HARV at all three span stations, but not on the ailerons at BL 191. Pressure distributions were obtained at all three span stations on the left wing and only at the midspan station on the right. In general the data showed very good agreement. Suction peaks at the leading edge were noted at the inboard station, indicating that the leading-edge flow is still attached. At the outboard station the flat pressure distribution and trailing-edge pressure deficit indicate extensive separated flow. This is in agreement with inflight flow visualization at $\alpha \approx 30°$, in which tufts showed attached chordwise flow near the inboard station on the leading-edge flap and reversed flow was shown near the outboard station. The tufts also showed significant spanwise flow near the two inboard stations over the main wing and reversed flow near the outboard station. Similar flow visualization results were observed in the wind-tunnel experiment using flow cones and tufts.
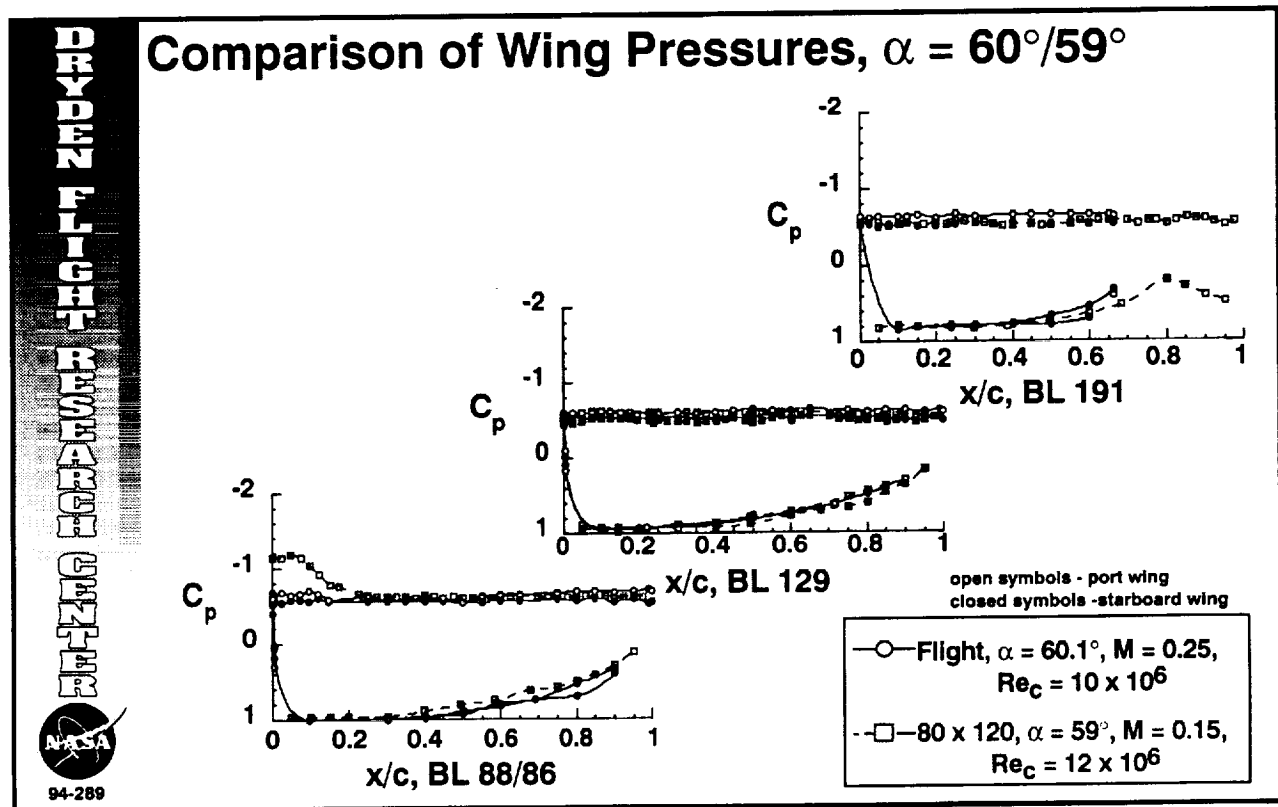

Comparison of Wing Pressures, $\alpha = 30°$

open symbols - port wing
closed symbols - starboard wing

—○—Flight, $\alpha = 29.9°$, M = 0.26, $Re_c = 10 \times 10^6$

--□--80 × 120, $\alpha = 30°$, M = 0.15, $Re_c = 12 \times 10^6$

94-287
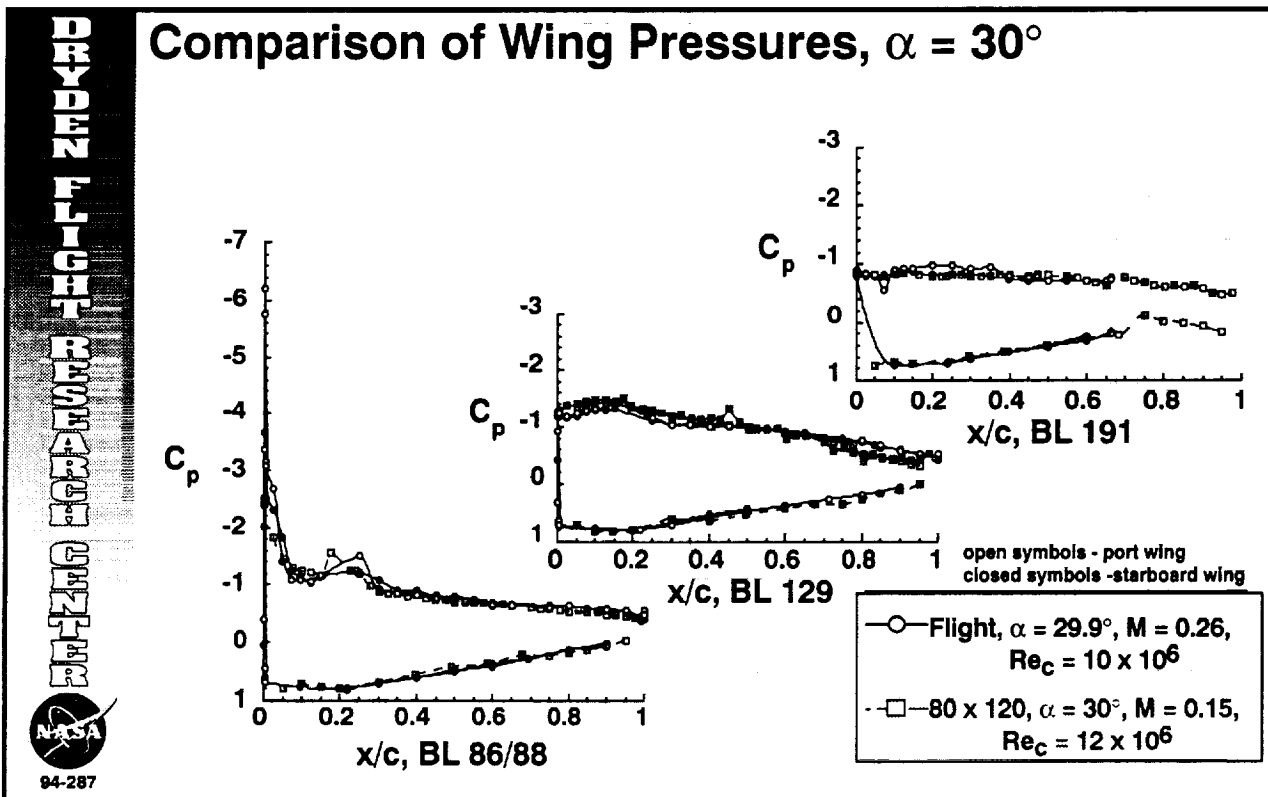
Wing, $\alpha = 45°$

At $\alpha = 45°$ the pressure distributions from both flight and wind tunnel show very good agreement. The flat pressure distributions and trailing-edge deficits indicate extensively separated flow over the entire wing. A comparison of the externally mounted pressure orifices on the starboard wing with the flush orifices on the port wing of the F/A-18 was made. The root-mean-square of the difference between the flush-measured pressure coefficients and the externally measured coefficients was approximately 0.1, with the externally measured pressure coefficients tending to be slightly more negative than those for the flush orifices. This is in good agreement with reference 17 for a similar installation at Mach numbers of 0.5, 0.9, and 0.97.

Comparison of Wing Pressures, $\alpha = 45°$

open symbols - port wing
closed symbols - starboard wing

—O— Flight, $\alpha = 44.8°$, M = 0.23, $Re_c = 9 \times 10^6$

-□- 80 x 120, $\alpha = 45°$, M = 0.15, $Re_c = 12 \times 10^6$

94-288

Wing, $\alpha = 60°/59°$

Wing pressure distributions shown in the figure were obtained in flight at $\alpha = 60°$ and in the wind tunnel at $\alpha = 59°$. The flight and wind-tunnel results show very good agreement at the two outboard stations with very flat pressure distributions and an average pressure coefficient of ≈ -0.6. At BL 88, the wind-tunnel data show a suction peak on the leading-edge flap that the flight data do not show. The wind-tunnel data were obtained without engines allowing airflow through the inlets and through the exhaust while the flight data were obtained with the engines at military power setting. To further examine the effects of no engines, these conditions were simulated in the NASA Dryden water tunnel. For the wind-tunnel simulation with flow through inlets and open exhaust, a vortex emanating from the inboard corner of the leading-edge flap traveled spanwise across the orifice station. In the flight simulation, with the mass flow of the engines simulated, the leading-edge flap vortex was much more chordwise and farther from the flap surface.

Comparison of Wing Pressures, $\alpha = 60°/59°$

open symbols - port wing
closed symbols - starboard wing

—○—Flight, $\alpha = 60.1°$, M = 0.25, $Re_c = 10 \times 10^6$

--□—80 x 120, $\alpha = 59°$, M = 0.15, $Re_c = 12 \times 10^6$

94-289

Summary

Pressure distributions obtained from the forebody, leading-edge extensions (LEXs) and wings obtained in flight from the F-18 HARV at NASA Dryden Flight Research Center were correlated with similar pressure distributions obtained on an F/A-18 in the NASA Ames Research Center's 80- x 120-ft wind tunnel. Pressure distributions were obtained at five circumferential rings on the forebodies and spanwise rows at three fuselage stations on both the LEXs. Pressure distributions were also obtained at three span stations on both wings in flight while pressure distributions were obtained at the nearly identical station on the left wing but only the midspan station on the right wing. The following results were observed.

At $\alpha = 30°$ the pressure distributions obtained on the forebody and wings in the wind tunnel were in excellent agreement with those obtained in flight. The pressure distributions obtained on the LEX, however, were not in agreement because of an effect of Mach number.

At $\alpha = 45°$ the forebody pressure distributions from the wind tunnel had larger suction peaks than those from flight. The pressure distributions for the LEX from both wind tunnel and flight were in good agreement with the flight data indicating unsteady pressures at the aft station. Data from the wing were in very good agreement and indicated extensive separated flow by the flat pressure distributions and pressure deficit at the trailing edge.

At $\alpha = 60°$ the asymmetries were noted in the pressure distributions from both the wind tunnel and flight. On the LEX large pressure fluctuations were observed in the flight data, and the wind-tunnel data generally fell within those bounds. The pressure distributions from the wings were flat and extensively separated except for the leading-edge flap at the inboard station for the wind tunnel. It is postulated that because of the difference in inlet flow between wind tunnel and flight, a vortex from the corner of the leading-edge flap sweeps over this location causing a suction peak in the wind-tunnel case.

Summary

- At $\alpha = 30°$, forebody and wing pressure distributions in excellent agreement; effect of Mach number present at LEX

- At $\alpha = 45°$, suction peaks in the forebody pressure distribution were larger than in flight; LEX and wing pressure distributions in good agreement; extensive separated flow on wings

- At $\alpha = 60°/59°$, forebody asymmetries were noted for both flight and wind-tunnel pressure distributions; unsteady pressures noted in flight; lack of simulated engine flow affected flow over inboard leading edge flap in wind tunnel

DRYDEN FLIGHT RESEARCH CENTER

94-290

References

1. Gilbert, William P., Luat T. Nguyen, and Joseph Gera, "Control Research in the NASA High-Alpha Technology Program," in *Aerodynamics of Combat Aircraft Controls and of Ground Effects*, AGARD CP-465, paper #3, 1990.

2. Regenie, Victoria, Donald Gatlin, Robert Kempel, and Neil Matheny, *The F-18 High Alpha Research Vehicle: A High-Angle-of-Attack Testbed Aircraft*, NASA TM-104253, Sept. 1992 (also published as AIAA 92-4121).

3. Murri, Daniel G., Gautam H. Shah, Daniel J. DiCarlo, and Todd. W. Trilling, "Actuated Forebody Strake Controls for the F-18 High Alpha Research Vehicle," AIAA 93-3675, Aug. 1993.

4. Lanser, Wendy R. and Daniel G. Murri, "Wind Tunnel Measurements on a Full-Scale F/A-18 with Forebody Slot Blowing or Forebody Strakes," AIAA 93-1018, Feb. 1993.

5. Fisher, David F., John H. Del Frate, and David M. Richwine, *In-Flight Flow Visualization Characteristics of the NASA F-18 High Alpha Research Vehicle at High Angles of Attack*, NASA TM-4193, May 1990.

6. Fisher, David F., Daniel W. Banks, and David M. Richwine, *F-18 High Alpha Research Vehicle Surface Pressures: Initial In-Flight Results and Correlation With Flow Visualization and Wind-Tunnel Data*, NASA TM-101724, Aug. 1990. (Also available as AIAA 90-3018.)

7. Ghaffari, Farhad, James M. Luckring, James L. Thomas, Brent L. Bates, and Robert T. Biedron, "Multiblock Navier-Stokes Solutions About the F/A-18 Wing-LEX-Fuselage Configuration," *J. Aircraft*, vol. 30, no. 3, May–June 1993, pp. 293–303.

8. Rizk, Yehia M. and Ken Gee, "Unsteady Simulation of Viscous Flowfield Around F-18 Aircraft at Large Incidence," *J. Aircraft*, vol. 29, no. 6, Nov.–Dec. 1992, pp. 986–992.

9. Erickson, G. E., R. M. Hall, D. W. Banks, J. H. Del Frate, J. A. Schreiner, R. J. Hanley, and C. M. Pulley, "Experimental Investigation of the F/A-18 Vortex Flows at Subsonic Through Transonic Speeds, Invited Paper," AIAA 89-2222, July–Aug. 1989.

10. Hall, R. M. and D. W. Banks, "Progress in Developing Gritting Techniques for High Angle of Attack Flows," AIAA 94-0169, Jan. 1994.

11. Banks, Daniel W., Robert M. Hall, Gary E. Erickson, and David F. Fisher, "Forebody Flow Field Effects on the High Angle-of-Attack Lateral-Directional Aerodynamics of the F/A-18," AIAA-94-0170, Jan. 1994.

12. James, K. D. and L. A. Meyn, "Dependence of Integrated Vertical-Tail Buffet Loads for F/A-18 on Sensor Density," SAE 941140, Apr. 1994.

13. Meyn, Larry A., Wendy R. Lanser, and Kevin D. James, "Full-Scale High Angle-of-Attack Tests of an F/A-18," AIAA 92-2676, June 1992.

14. Rae, William H., Jr., and Alan Pope, *Low-Speed Wind Tunnel Testing*, Second Edition, John Wiley & Sons, New York, 1984.

15. Fisher, David F. and Brent R. Cobleigh, *Controlling Forebody Asymmetries in Flight—Experience With Boundary Layer Transition Strips*, NASA TM- 4595, July 1994. (Also available as AIAA 94-1826.)

16. Del Frate, John H. and Fanny A. Zuniga, "In-Flight Flow Field Analysis on the NASA F-18 High Alpha Research Vehicle With Comparisons to Ground Facility Data," AIAA 90-0231, Jan. 1990.

17. Montoya, Lawrence C. and David P. Lux, *Comparisons of Wing Pressure Distribution from Flight Tests of Flush and External Orifices for Mach Numbers from 0.50 to 0.97*, NASA TM X-56032, Apr. 1975.